International Journal of Nanomedicine

Dovepress
Taylor & Francis Group

Open Access Full Text Article

ORIGINAL RESEARCH

Quercetin-Loaded Nanoparticle-Modified Decellularized Tissue-Engineered Vascular Graft Regulates Macrophage Polarization and Promotes In Vivo Graft Remodeling

Tun Wang[1,2,*], Zhenyu He[1,2,*], Peng Lu[1,2], Sheng Liao[1,2], Siyuan Cheng[1,2], Tianjian Wang[1,2], Yangyang An[1,2], Zibo Cheng[1,2], Chang Shu[1–3]

[1]Department of Vascular Surgery, the second Xiangya Hospital, Central South University, Changsha, 410011, People's Republic of China; [2]Institute of Vascular Diseases, Central South University, Changsha, 410011, People's Republic of China; [3]Center of Vascular Surgery, Fuwai Hospital, Chinese Academy of Medical Sciences and Peking Union Medical College, Beijing, 100037, People's Republic of China

*These authors contributed equally to this work

Correspondence: Chang Shu, Email changshu_vascular@163.com

Introduction: Arteriovenous graft (AVG) is an important option for establishing hemodialysis access in patients with end-stage chronic kidney disease (CKD). Decellularized tissue-engineered vascular graft (dTEVG), due to its excellent biocompatibility and regenerative potential, holds promise for use in AVG; however, poor remodeling remains a challenge. Quercetin (Qu) can effectively regulate macrophage polarization and promote tissue remodeling and regeneration, yet its low bioavailability limits its clinical application.

Methods: Here, we developed a nano-localized drug delivery system using Qu-loaded poly(lactic-co-glycolic acid) (PLGA) nanoparticles (Qu@PNPs), prepared via a nanoprecipitation method and subsequently modified onto the surface of dTEVG. In vitro and in vivo experiments were performed to assess the biocompatibility of Qu@PNPs and their effect on macrophage polarization. Additionally, the impact of Qu@PNPs modification on dTEVG remodeling was evaluated in both subcutaneous and AVG rat models.

Results: Our study results demonstrated that Qu@PNPs exhibited good biocompatibility and achieved sustained drug release on dTEVG. Furthermore, these drug-loaded nanoparticles inhibited M1 macrophage polarization while promoting M2 polarization, significantly improving the in vivo remodeling of dTEVG, as evidenced by increased early recellularization and peripheral neovascularization.

Conclusion: Together, the development of the nano-localized drug delivery system effectively enhanced the application of Qu, providing experimental evidence for its use in dTEVG. Additionally, it offers new strategies and approaches for optimizing dTEVG design and clinical translation.

Keywords: arteriovenous graft, decellularized tissue-engineered vascular graft, macrophage polarization, nanoparticles, quercetin, graft remodeling

Introduction

Chronic kidney disease (CKD) has become an increasingly serious public health issue worldwide.[1,2] Most end-stage CKD patients rely heavily on hemodialysis as their primary renal replacement therapy, with reliable vascular access being crucial for successful treatment.[3–5] The arteriovenous graft (AVG) is an essential alternative for hemodialysis treatment.[4,6] Synthetic grafts are currently the preferred option for constructing AVG in clinical practice, primarily made from expanded polytetrafluoroethylene (ePTFE) and Dacron.[7] However, their use is often associated with complications such as infection, thrombosis, and intimal hyperplasia.[8,9] In light of these limitations, decellularized tissue-engineered

Received: 11 November 2024
Accepted: 26 February 2025
Published: 5 March 2025

vascular graft (dTEVG), which offers superior biocompatibility and regenerative potential, represent a promising alternative solution.

Over the past few decades, dTEVG constructed from decellularized natural vascular tissue has gained increasing attention due to their low immunogenicity and retention of natural vascular structures.[10–12] An ideal dTEVG can support host cell growth and regenerate a bioactive vascular structure resembling native blood vessels.[13,14] However, studies have shown that dTEVG still faces challenges such as insufficient recellularization and poor remodeling during in vivo adaptation.[15–17] Good recellularization in AVG is crucial for restoring the biological function of acellular grafts in hemodialysis, as the risk of graft rupture, pseudoaneurysm, thrombosis, stenosis, and infection significantly increases after repeated punctures.[18,19]

Quercetin (Qu), a naturally occurring flavonoid that is widely available and can be synthesized in vitro, has been found to regulate macrophage polarization by primarily inhibiting M1 polarization and promoting M2 polarization.[20–23] Recent studies have shown that macrophage polarization plays a crucial role in graft remodeling.[24,25] However, whether Qu regulates dTEVG remodeling remains unclear. Moreover, Qu's clinical application has been limited by its poor chemical stability and low water solubility.[26,27] To address these limitations, we designed a localized drug delivery system based on poly(lactic-co-glycolic acid) (PLGA) nanoparticles (PNPs). Specifically, drug-loaded PNPs were prepared using the nanoprecipitation method.[28] The carboxyl groups on the nanoparticle surface were then activated via 1-Ethyl-3-(3-dimethylaminopropyl)carbodiimide (EDC)/N-Hydroxy succinimide (NHS) chemical coupling and conjugated with the amino groups on the surface of dTEVG to form stable amide bonds, thereby successfully constructing the localized drug delivery system.[29] Among them, PLGA was selected as the drug carrier due to its excellent biocompatibility, controlled degradation properties, and favorable drug loading and sustained release capabilities.[30,31]

In summary, through this study, we aim to reveal Qu's potential in improving dTEVG remodeling, explore the relationship between Qu, macrophage polarization, and graft remodeling, and provide new insights and strategies for the further optimization and application of dTEVG.

Material and Methods

Preparation and Characterization of Nanoparticles

PLGA (Sigma-Aldrich, St. Louis, USA) was selected as the substrate for the nanoparticles. Qu-loaded PNPs (Qu@PNPs) were prepared using the nanoprecipitation method.[28,32] In brief, an appropriate amount of Qu (Sigma-Aldrich) was dissolved in 5 mL of acetone (Aladdin, Shanghai, China), and 3 mL of this solution was mixed with 30 mg of PLGA in the organic phase. Meanwhile, polyvinyl alcohol (PVA) (Aladdin) was dissolved in pure water to prepare 1% (w/v) PVA aqueous phase. The organic phase was slowly injected into the aqueous phase at a volume ratio of 1:10. The mixture was stirred at a constant speed for 30 minutes in an ice bath, then the acetone was removed under reduced pressure to obtain a nanoparticle suspension. The nanoparticle suspension was centrifuged at 21,130 ×g for 15 minutes and washed three times to thoroughly remove impurities. The purified nanoparticles were then freeze-dried and stored at 4°C. Drug-free PNPs were prepared using the same method. Additionally, Rhodamine B (Sigma-Aldrich)-loaded PNPs (RB@PNPs) were synthesized for subsequent fluorescence visualization of the nanoparticles.

The particle size and zeta potential of PNPs and Qu@PNPs were measured using a nano-ZS90 dynamic light scattering (DLS) particle size analyzer (Malvern, Shanghai, China). The detection methods for particle size and zeta potential were conducted according to the specifications of the Zetasizer software. In brief, the nanoparticle suspension was diluted with pure water to the working concentration. One milliliter of the diluted sample was placed in a cuvette for particle size measurement, while an equal amount of the sample was used in the zeta potential cell for zeta potential assessment.

The morphology of PNPs and Qu@PNPs was observed using a transmission electron microscope (TEM) (HITACHI, Tokyo, Japan). The procedure was as follows: First, 20 μL of the nanoparticle suspension was pipetted onto a carbon-coated copper grid and left for 3–5 minutes to allow excess liquid to be absorbed with filter paper. Next, 2% phosphotungstic acid (Servicebio, Wuhan, China) was applied to the carbon support film for 1–2 minutes, and excess

liquid was again removed with filter paper, followed by drying at room temperature. Finally, the samples were observed under TEM.

Drug loading measurement of the nanoparticles: An accurate weight of 10 mg of Qu@PNPs lyophilized powder was dispersed in 5 mL of distilled water. Then, 200 μL of the suspension was precisely transferred into 1.8 mL of methanol (Aladdin, Shanghai, China) and thoroughly vortexed to disrupt the nanoparticle structure and release the drug components. The absorbance of Qu at the maximum wavelength of 374 nm was measured using a multifunctional microplate reader (Huisong, Shenzhen, China), and the Qu content was calculated based on the corresponding standard curve formula. Finally, the drug loading was calculated using the following formula: Drug loading (%) = (Mass of drug in nanoparticles / Total mass of drug-loaded nanoparticles) × 100%, resulting in a Qu loading of approximately 4.04 ± 0.16%.

Drug encapsulation efficiency measurement of the nanoparticles: The Qu content in the drug-loaded nanoparticles was determined using the previously described method. Encapsulation efficiency was calculated using the following equation: Drug encapsulation efficiency (%) = (Mass of drug in nanoparticles / Total mass of drug added) × 100%. The encapsulation efficiency of the nanoparticles was calculated as 64.89 ± 0.22%.

Stability of Nanoparticles

At various time points (day 0, 1, 3, 5, 7, and 14), an appropriate amount of lyophilized nanoparticle powder was taken out and thoroughly mixed in pure water, then diluted to the working concentration for particle size and zeta potential measurements. This was done to evaluate the stability of nanoparticle size and zeta potential over time. Additionally, equal amounts of Qu@PNPs lyophilized powder were collected at the same time points, and drug loading was measured using the previously described method to assess the stability of drug loading in the nanoparticles over time.

Preparation and Characterization of dTEVG

The dTEVG was derived from natural vascular tissue. The natural vascular tissue was obtained from the common carotid arteries of local ducks, which were sourced from a local slaughterhouse and had an average body weight of approximately 1500 g. The decellularization procedure was performed according to previous studies.[33] In brief, a comprehensive decellularization protocol combining physical, chemical, and biological methods was employed: First, the 1.5 cm long duck carotid artery was subjected to freeze-thaw cycles at −20°C. It was then incubated for 12 hours in a 3-[(3-cholamidopropyl)dimethylammonium]-1-propanesulfonate (CHAPS) buffer (8 mM CHAPS [Sigma–Aldrich],1 M NaCl [Sigma–Aldrich], and 25 mM Ethylenediaminetetraacetic acid (EDTA) [Sigma–Aldrich] in phosphate buffered solution (PBS) [Sigma–Aldrich]), followed by a 24-hour incubation in a Sodium dodecyl sulfate (SDS) buffer (1.8 mM SDS [Sigma–Aldrich], 1 M NaCl, and 25 mM EDTA in PBS). After incubation, the artery was washed in clean PBS for 24 hours. Finally, treatment with DNase I (3000 U/mL) (Sigma-Aldrich) and RNase A (3000 U/mL) (Sigma-Aldrich) for 1 hour completed the decellularization process.

Some sections of the blood vessels before and after decellularization were embedded in paraffin and sliced into approximately 4 μm thick sections for storage. After undergoing a series of steps, including baking, deparaffinization, and dehydration, the tissue sections were stained with Hematoxylin-Eosin (HE) and 4',6-diamidino-2-phenylindole (DAPI) (Sigma-Aldrich) to evaluate the success of the decellularization process.

Modification and Testing of dTEVG

The dTEVG was surface modified using the EDC/NHS method. The procedure is as follows: First, PNPs or Qu@PNPs were activated by adding them to an activation buffer containing 10 μmol/mL EDC (Sigma-Aldrich) and 10 μmol/mL NHS (Sigma-Aldrich) in 0.1 M 2-Morpholinoethanesulphonic acid (MES) (Sigma-Aldrich) buffer (pH 5.0) to activate the carboxyl groups for 1 hour. The activated PNPs or Qu@PNPs were then centrifuged and washed with PBS. Next, they were resuspended in a reaction buffer at approximately pH 8.0, prepared using 1 M NaOH in PBS, and a 1.5 cm long dTEVG was added to the reaction buffer and incubated overnight at 37°C in the dark. To ensure consistency in control experiments, Qu alone underwent the same treatment for "mock modification" with an equal length of dTEVG. Ultimately, three groups of modified dTEVG were obtained: PNPs-dTEVG, Qu@PNPs-dTEVG, and Qu-dTEVG, with

unmodified dTEVG serving as the blank control. Additionally, RB@PNPs for fluorescent visualization were modified onto the surface of dTEVG using the aforementioned method, resulting in the formation of the RB@PNPs-dTEVG group.

The microscopic morphology of dTEVG before and after modification was observed using a scanning electron microscope (SEM) (TESCAN, Czech Republic) to detect surface structure changes. The detection method involved fixing the samples in 2.5% (v/v) glutaraldehyde (Sigma-Aldrich) for 12 hours, followed by dehydration in a series of ascending ethanol concentrations. The samples were then mounted on aluminum stubs, sputter-coated with gold, and observed under SEM. Additionally, macroscopic observations of dTEVG before and after modification were conducted.

Drug Release Profile

In vitro drug release studies were conducted in PBS solution at pH 7.4 containing 1% polyethylene glycol-400 (PEG-400) (Sigma-Aldrich). In brief, the modified dTEVG was washed and placed in the PBS solution, then stored in the dark at 37°C. Starting from day 0, an equal volume of supernatant was taken every two days and frozen at −80°C for later analysis, while an equal volume of fresh PBS solution was added to continue the incubation at 37°C. The amount of drug was measured as previously described, using a multifunctional microplate reader to detect the absorbance of Qu at the maximum wavelength of 374 nm, and the Qu content in the supernatant was calculated based on the corresponding standard curve formula.

Cell Viability Assessment

Cell viability was assessed using the Cell Counting Kit-8 (CCK-8) (Beyotime, Shanghai, China) to evaluate the effects of Qu and nanoparticles on rat bone marrow-derived macrophages (BMDMs). Rat BMDMs were previously extracted, and the culture medium used was dulbecco's modified eagle medium (DMEM) (Thermo Fisher Scientific, Massachusetts, USA) supplemented with 10% fetal bovine serum. The experimental steps are as follows: rat BMDMs were treated with a series of Qu concentrations (0, 1.25, 2.5, 5, 10, 20, 40, and 80 μM) for 24 hours. After changing the culture medium, cell viability was assessed using the CCK-8 method. Additionally, another group of Qu-treated cells was stained with crystal violet to observe viable cells. Subsequently, based on the results of the previous tests, an appropriate concentration of Qu was selected for the preparation of Qu@PNPs. The prepared Qu@PNPs were used to treat cells at a series of mass concentrations of 0, 10, 50, 100, 200, and 300 μg/mL, following the same time and method as previously described. Additionally, a blank control group (Control) and a PNPs group with the same concentration gradient were routinely set up to exclude the influence of the nanoparticles themselves. This approach aimed to determine whether the drug-loaded nanoparticles affect cell viability within a certain concentration range and to establish an appropriate nanoparticle amount for graft modification in subsequent in vivo experiments.

Macrophage Polarization Assessment

In vitro, rat BMDMs were used to investigate the effect of 40 μM Qu on macrophage polarization. The experimental groups included control, Qu, lipopolysaccharide (LPS) (Beyotime), and LPS+Qu. The treatments were as follows: the Qu and LPS groups received individual interventions for 24 hours, while the LPS+Qu group was treated with Qu for 30 minutes before LPS (100 ng/mL) was added, continuing for 24 hours. Macrophage polarization was assessed by Western blot (WB) and immunofluorescence. Next, the effect of Qu@PNPs (with approximately 40 μM Qu) on macrophage polarization was evaluated, with the same experimental groups, plus a PNPs-only group to control for nanoparticle effects. The treatment and analysis procedures were the same as above, with polarization detected by immunofluorescence.

In vivo experiments followed the animal grouping scheme, and at the endpoint, tissue samples were collected and sectioned for immunofluorescence to evaluate macrophage polarization in tissues.

Western Blot

Total protein was extracted from cells using radioimmunoprecipitation assay (RIPA) lysis buffer (Beyotime) and protein concentrations were determined using a colorimetric method. For immunoblotting, proteins (20–40 μg) were separated

on 8%-10% sodium dodecyl sulfate-polyacrylamide gel electrophoresis (SDS-PAGE) gels (Epizyme, Shanghai, China) and transferred to a microporous membrane (0.45 μm; Immobilon, Millipore) by electrophoresis. The membrane was blocked with 5% bovine serum albumin (BSA) (Epizyme) at room temperature for 1 hour, followed by overnight incubation with the primary antibody against the target protein at 4°C. Afterward, the membrane was incubated with a horseradish peroxidase-conjugated secondary antibody at room temperature for 1 hour, and developed using enhanced chemiluminescence (ECL) reagents (Epizyme). If necessary, stripping buffer was used to elute the antibodies, and the membrane was treated again as described.

The primary antibodies used in this experiment included: anti-inducible nitric oxide synthase (iNOS) (Abcam, ab178945, 1:1000), anti-arginase-1 (Arg-1) (Proteintech, 16001-1-AP, 1:5000), and anti-β-actin (Proteintech, 20536-1-AP, 1:1000). The secondary antibody was Rabbit anti-IgG (Abclonal, AS014, 1:5000).

Animal Models

All experiments were approved by the Animal Care and Use Committee of the Second Xiangya Hospital of Central South University (Approval No. 20241053). All experiments were performed in accordance with the National Institutes of Health Guide for the Care and Use of Laboratory Animals. Male Sprague-Dawley (SD) rats at 11 weeks of age were selected for modeling.

Subcutaneous Implantation Model: Rats were anesthetized using inhaled isoflurane (RWD, China), and a longitudinal skin incision was made approximately 1.0 cm away from the spine on the back. Four groups of grafts—unmodified dTEVG (blank control), PNPs-dTEVG, Qu-dTEVG, and Qu@PNPs-dTEVG—were implanted subcutaneously, with one dTEVG implanted per rat. The skin was sutured using 3–0 surgical sutures. Post-surgery, the wound was disinfected, and the rats were monitored under standard housing conditions. The entire surgical procedure adhered to aseptic principles. After 21 days, the rats were euthanized, and tissue samples were collected. The sample size for each group was n=5.

AVG Model: The rat carotid artery-jugular vein AVG model requires advanced vascular surgical techniques. The surgical methods and specific steps followed were based on previous studies.[33] Four groups of different modified, equal-sized dTEVG (as used in the subcutaneous model) were connected between the carotid artery and jugular vein. After 21 days post-surgery, the rats were euthanized, and tissue samples were collected. The sample size for each group was n=5.

It is important to note that, in this surgical model, the three groups of modified dTEVG, except for the blank control group, maintained a consistent dosage of nanoparticles or drugs. Additionally, RB@PNPs-dTEVG was also used in the AVG model to observe the presence of nanoparticles within the graft under in vivo blood flow conditions.

Histology

Tissue samples obtained from the experiment were washed with PBS and then fixed in 4% paraformaldehyde (Biosharp, Hefei, China). Following fixation, the tissues were dehydrated in a series of graded ethanol concentrations. After dehydration, they were cleared in xylene and subsequently embedded in paraffin to form wax blocks. The tissue blocks were cut into 4 μm thick sections and placed on glass slides for storage. HE staining kit (Servicebio) was used to evaluate tissue morphology.

Immunofluorescence

Cell Immunofluorescence: Cells were fixed with 4% paraformaldehyde, blocked with 10% goat serum, and incubated with primary antibody overnight at 4°C. After washing, fluorescent secondary antibodies were applied for 1 hour, followed by DAPI staining. Observations were made using a fluorescence microscope (ZEISS, Oberkochen, Germany).

Tissue Immunofluorescence: Tissue sections were deparaffinized, followed by antigen retrieval in pH 9.0 Tris-EDTA buffer (Sigma-Aldrich) at 100°C for 20 minutes. After blocking nonspecific binding with 10% goat serum (1 hour, room temperature), sections were incubated with primary antibodies overnight at 4°C and secondary antibodies for 1 hour. Nuclei were counterstained with DAPI, and sections were mounted. Observations were conducted using a fluorescence microscope.

The primary antibodies used in this experiment included: anti-Cluster of Differentiation 68 (CD68) (Abcam, ab31630, 1:400), anti-iNOS (Abcam, ab178945, 1:200), anti-CD206 (Abcam, ab64693, 1:200), anti-CD31 (AiFang, AF6408,

1:50), and anti-alpha smooth muscle actin (α-SMA) (Proteintech, 67735-1-Ig, 1:200). The secondary antibodies included Fluorescein Isothiocyanate (FITC)-conjugated Goat anti-Rabbit (Proteintech, SA0003-2, 1:200) and Sulfo-Cyanine3 (Cy3)-conjugated Goat anti-Mouse (Proteintech, SA0009-1, 1:200).

Cell Counting Within the Graft

The grafts were collected on postoperative day 21 (n=5) and processed into paraffin blocks using the previously described histological methods. Cross-sections of 4 μm thickness were cut from the middle portion of the graft. The cell nuclei were stained using DAPI fluorescence (blue), and tissue autofluorescence was appropriately exposed to distinguish the structures. Under a fluorescence microscope, the medial region of the entire tubular graft was identified, with the internal and external elastic laminae marked using white dashed lines. The cell counting within the graft was performed within the annular region between the white dashed lines. All experiments were independently counted by two or more researchers, and the average value was taken to ensure the accuracy and consistency of the results.

Counting of Peripheral New Blood Vessels

The grafts were collected on postoperative day 21 (n=5) and processed into paraffin blocks using the previously described histological methods. Cross-sections of 4 μm thickness were cut from the middle portion of the graft. The surrounding new blood vessels of the graft were stained using CD31 (green) and α-SMA (red) fluorescence, with tissue autofluorescence appropriately exposed to distinguish the structures. Under a fluorescence microscope, the adventitial region of the entire tubular graft, at a fixed distance from the external elastic lamina, was identified, and the CD31-positive or CD31 and α-SMA double-positive annular structures in this region were counted. All experiments were independently counted by two or more researchers, and the average value was taken to ensure the accuracy and consistency of the results.

Statistical Analysis

Data are represented as mean value ± standard error of the mean. All data were analyzed using Prism 10 software (GraphPad Software, Inc., La Jolla, CA). Between-group comparisons will be conducted using one-way analysis of variance (ANOVA), and post hoc tests (such as Tukey's HSD test) will be performed to identify specific differences when significant differences are observed. Multifactorial ANOVA will be applied for comparisons involving two or more factors. For non-normally distributed data, non-parametric tests (such as the Mann–Whitney *U*-test) will be utilized. Correlation analyses will employ either Pearson or Spearman correlation coefficients, depending on the distribution of the data. P values < 0.05 were considered significant.

Results

Preparation and Characterization of Nanoparticles

The preparation of Qu@PNPs was carried out using the nanoprecipitation method, involving steps such as oil-water phase mixing, ice bath stirring, and solvent evaporation (Figure 1A). PNPs were prepared using the same procedure. The purified PNPs and Qu@PNPs were then lyophilized and stored in appropriate containers (Figure 1B). TEM analysis of PNPs and Qu@PNPs revealed smooth, spherical morphology, with the particle size of Qu@PNPs being slightly larger than that of PNPs (Figure 1C). DLS analysis showed that the particle size of PNPs was 177.7 ± 56.54 nm with a zeta potential of −31.6 ± 4.25 mV, while Qu@PNPs had a particle size of 249.0 ± 89.24 nm and a zeta potential of −32.7 ± 4.61 mV (Figure 1D). Additionally, some prepared PNPs and Qu@PNPs were stored at 4°C and periodically sampled to assess their stability. The results showed no significant changes in Z-average particle size and zeta potential over 14 days, indicating good stability under 4°C conditions (Figure 1E and F). Furthermore, the drug loading and encapsulation efficiency of Qu@PNPs were 4.04 ± 0.16% and 64.89 ± 0.22%, respectively. Notably, the drug loading remained stable after 14 days of storage at 4°C, further demonstrating the excellent stability of the nanoparticles prepared in this study (Figure 1G).

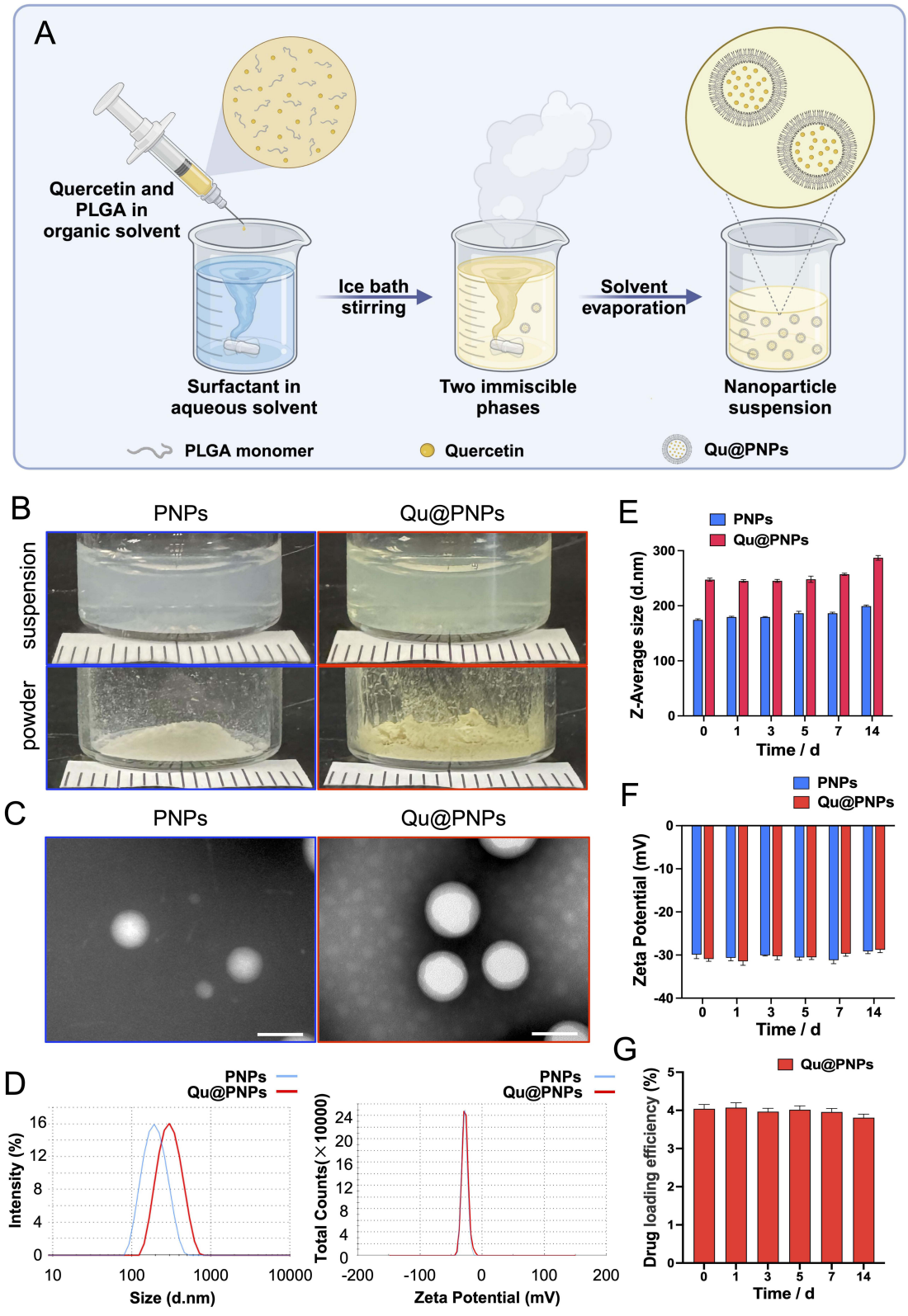

Figure 1 Preparation and characterization of Qu@PNPs. (**A**) Schematic diagram of the preparation process of Qu@PNPs (nanoprecipitation method). (**B**) Macroscopic appearance of PNPs and Qu@PNPs (suspension and lyophilized powder). (**C**) TEM images of PNPs and Qu@PNPs, scale bar: 200 nm. (**D**) Particle size and zeta potential distributions of PNPs and Qu@PNPs. (**E**) Z-average particle size stability of PNPs and Qu@PNPs over time (n=3). (**F**) Zeta potential stability of PNPs and Qu@PNPs over time (n=3). (**G**) Drug loading stability of Qu@PNPs over time (n=3). Data are presented as mean value ± standard error of the mean.

https://doi.org/10.2147/IJN.S505674

Construction and Characterization of Nanoparticles-dTEVG

Qu@PNPs-dTEVG was prepared through a series of steps, including the decellularization of natural blood vessels and covalent binding of nanoparticles (Figure 2A). Concurrently, both PNPs and Qu alone were modified onto the surface of dTEVG using the same construction process. The decellularization of natural carotid arteries involved a combination of physical, chemical, and biological methods, effectively removing the original cells from the tissue (Supplementary Figure 1). To confirm the successful modification of nanoparticles onto the surface of dTEVG, we conducted visual and SEM observations on four groups of differently treated dTEVG. Visually, the unmodified dTEVG group appeared more translucent compared to the PNPs-dTEVG group, while both the Qu-dTEVG and Qu@PNPs-dTEVG groups exhibited a light-yellow appearance. SEM analysis revealed numerous nanoparticles adhering to both the inner and outer surfaces of PNPs-dTEVG and Qu@PNPs-dTEVG, providing preliminary evidence for the successful modification of nanoparticles on the dTEVG surface (Figure 2B and C). Furthermore, to obtain more conclusive evidence, in vitro drug release experiments were performed on the four groups of dTEVG. The results indicated that the Qu@PNPs-dTEVG group exhibited a more sustained drug release capability compared to the Qu-dTEVG group, while the total amount of drug released in both groups was comparable (Figure 2D). Collectively, these findings demonstrate that the Qu@PNPs-dTEVG localized drug delivery system has been successfully constructed and possesses good drug release capabilities. Additionally, in the in vivo AVG model, 72 hours after the implantation of RB@PNPs-dTEVG, a considerable amount of red fluorescence signal (originating from RB@PNPs) was still observed in the adventitial region of the graft (Supplementary Figure 3).

Evaluation of the Biocompatibility of Qu@PNPs

To evaluate the biocompatibility of Qu@PNPs, both in vitro and in vivo experiments were conducted. In the in vitro experiments, we treated rat BMDMs with a series of Qu concentrations (0, 1.25, 2.5, 5, 10, 20, 40, and 80 μM) for 24 hours and performed crystal violet staining. Microscopic observations revealed a noticeable decrease in cell density at 80 μM (Figure 3A). The CCK-8 assay was then employed for quantitative analysis of cell viability, which demonstrated that Qu concentrations ranging from 0 to 40 μM did not adversely affect cell viability (Figure 3C). Therefore, the subsequent actual drug loading concentration of Qu@PNPs was set around 40 μM. Based on its drug-loading capacity, the corresponding mass concentration of Qu@PNPs was approximately 300 μg/mL. A series of mass concentrations of 0, 10, 50, 100, 200, and 300 μg/mL of Qu@PNPs were further prepared for 24-hour interventions. The Control group served as the blank control, and the PNPs group was subjected to the same concentration gradient to exclude the potential influence of nanoparticles. CCK-8 assay results showed that Qu@PNPs within this concentration range had no significant effect on cell viability (Supplementary Figure 2). Next, we further examined cell density after 24 hours in the control group, PNPs intervention group, Qu intervention group, and Qu@PNPs intervention group using crystal violet staining, combined with quantitative analysis of cell viability through the CCK-8 assay. The results indicated no significant changes in cell density or viability among the four groups (Figure 3B and D). For the in vivo experiments, unmodified dTEVG, PNPs-dTEVG, Qu-dTEVG, and Qu@PNPs-dTEVG were implanted into rats using the AVG model. On postoperative day 21, liver, kidney, and spleen samples were collected and examined using HE staining. No signs of inflammation or pathological changes were observed in the major organs of any group (Supplementary Figure 4). In summary, both in vitro and in vivo experiments demonstrated that the Qu@PNPs constructed in this study exhibit excellent biocompatibility.

In Vitro Regulation of Macrophage Polarization by Qu@PNPs

Previous studies have demonstrated that Qu can regulate macrophage polarization.[23,34] In this study, WB confirmed that Qu inhibited the polarization of rat BMDMs toward the pro-inflammatory M1 phenotype, as indicated by the suppressed expression of iNOS. The M1 macrophages were induced by LPS (Figure 4A and B). Additionally, WB analysis also verified that Qu promotes the polarization of rat BMDM towards the anti-inflammatory M2 phenotype, with significantly elevated levels of the M2 marker Arg-1 (Figure 4C and D). To further explore the effect of Qu@PNPs on macrophage polarization in vitro, Qu@PNPs were added to rat BMDMs and incubated for 24 hours. Microscopic observations

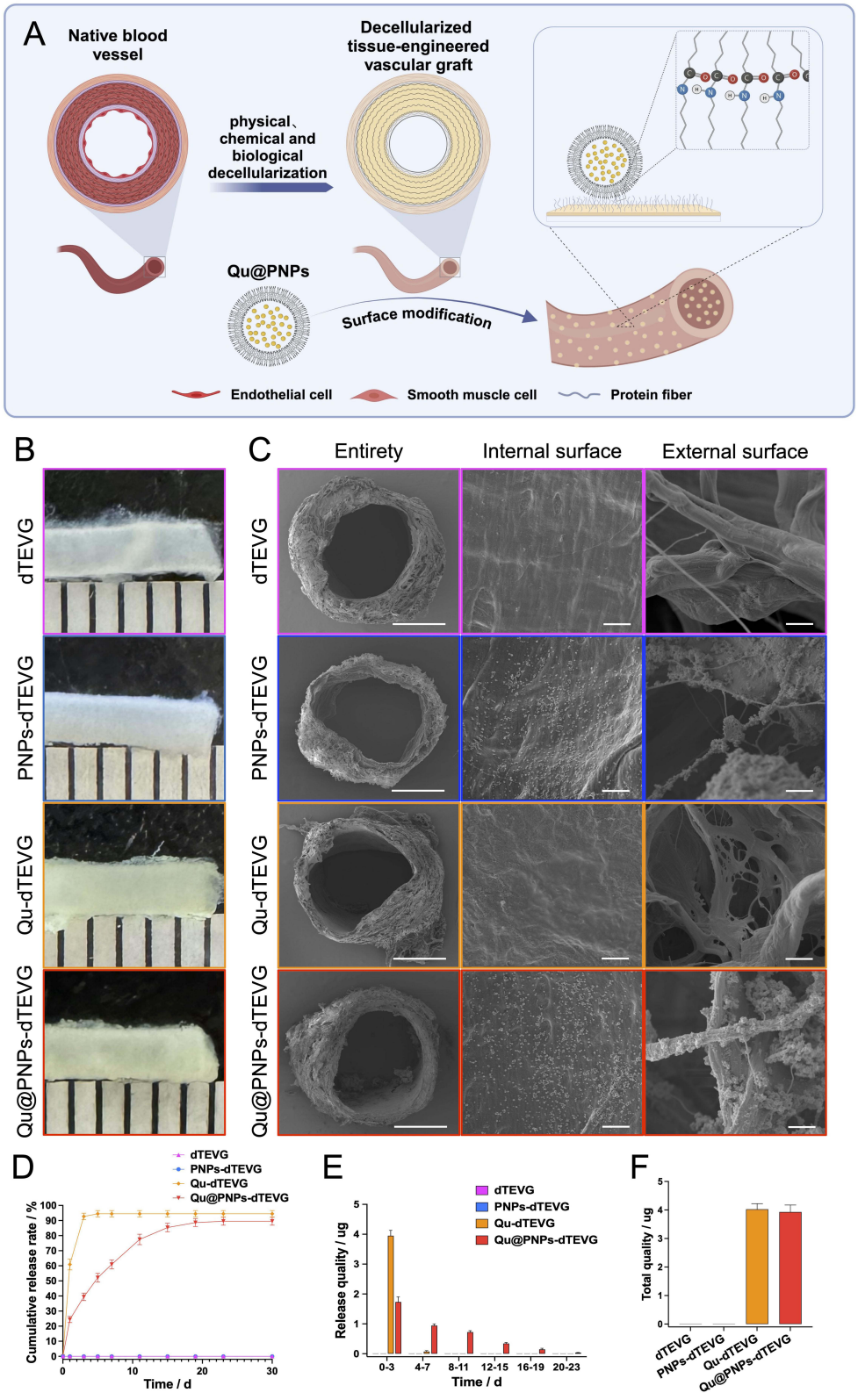

Figure 2 Construction and characterization of Qu@PNPs-dTEVG. (**A**) Schematic diagram of the decellularization of natural blood vessels and modification of dTEVG with Qu@PNPs. (**B**) Macroscopic appearances of dTEVG, PNPs-dTEVG, Qu-dTEVG, and Qu@PNPs-dTEVG. (**C**) SEM images of dTEVG, PNPs-dTEVG, Qu-dTEVG, and Qu@PNPs-dTEVG, with scale bars of 500 μm, 2 μm, and 2 μm (from left to right). (**D**) Cumulative drug release profiles of dTEVG, PNPs-dTEVG, Qu-dTEVG, and Qu@PNPs-dTEVG over time (n=3). (**E**) Absolute drug release profiles of dTEVG, PNPs-dTEVG, Qu-dTEVG, and Qu@PNPs-dTEVG over time at fixed intervals (n=3). (**F**) Total drug release amounts of dTEVG, PNPs-dTEVG, Qu-dTEVG, and Qu@PNPs-dTEVG (n=3). Data are presented as mean value ± standard error of the mean.

https://doi.org/10.2147/IJN.S505674

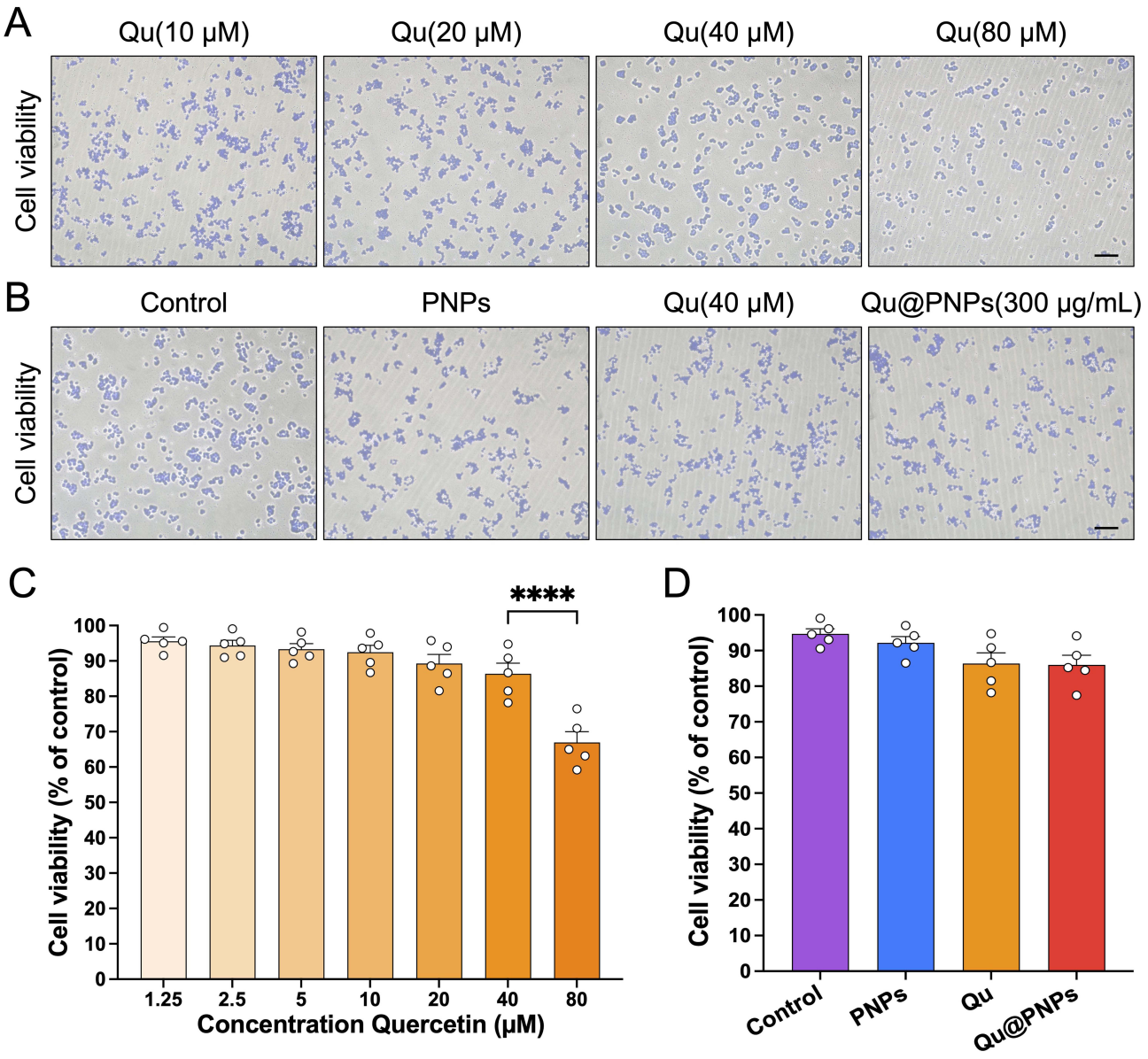

Figure 3 In vitro effects of Qu@PNPs on macrophage viability. (**A**) Microscopic images of rat BMDMs after 24 hours of treatment with different concentrations of Qu, with cell nuclei stained by crystal violet (blue), scale bar: 100 μm. (**B**) Microscopic images of rat BMDMs after 24 hours of intervention with different experimental groups, with cell nuclei stained by crystal violet (blue), scale bar: 100 μm. (**C**) Quantitative analysis of cell viability in rat BMDMs after 24 hours of intervention with gradient concentrations of Qu, measured by the CCK-8 assay (n=5). (**D**) Quantitative analysis of cell viability in rat BMDMs after 24 hours of intervention with different experimental groups, measured by the CCK-8 assay (n=5). Data are presented as mean value ± standard error of the mean, **** p<0.0001; ns: not significant (not shown in the figure).

revealed that both the Qu@PNPs and Qu intervention groups exhibited a similar "synaptic" morphology in a higher proportion of cells compared to other groups, suggesting that Qu@PNPs can influence macrophage polarization without being affected by the nanoparticle carrier (Figure 4E). Subsequently, cellular fluorescence detection was performed to evaluate the expression of the M1 marker iNOS and the M2 marker CD206 in macrophages, further confirming that Qu@PNPs inhibit the polarization of rat BMDMs toward M1 while promoting polarization toward M2 (Figure 4F-I).

Qu@PNPs Regulate Macrophage Polarization and Promote Early Recellularization and Peripheral Neovascularization of dTEVG in the Subcutaneous Model

Previous in vitro experiments demonstrated that Qu@PNPs significantly regulate macrophage polarization, inhibiting M1 macrophages while promoting M2 macrophages (Figure 4F-I). This finding lays the groundwork for investigating the

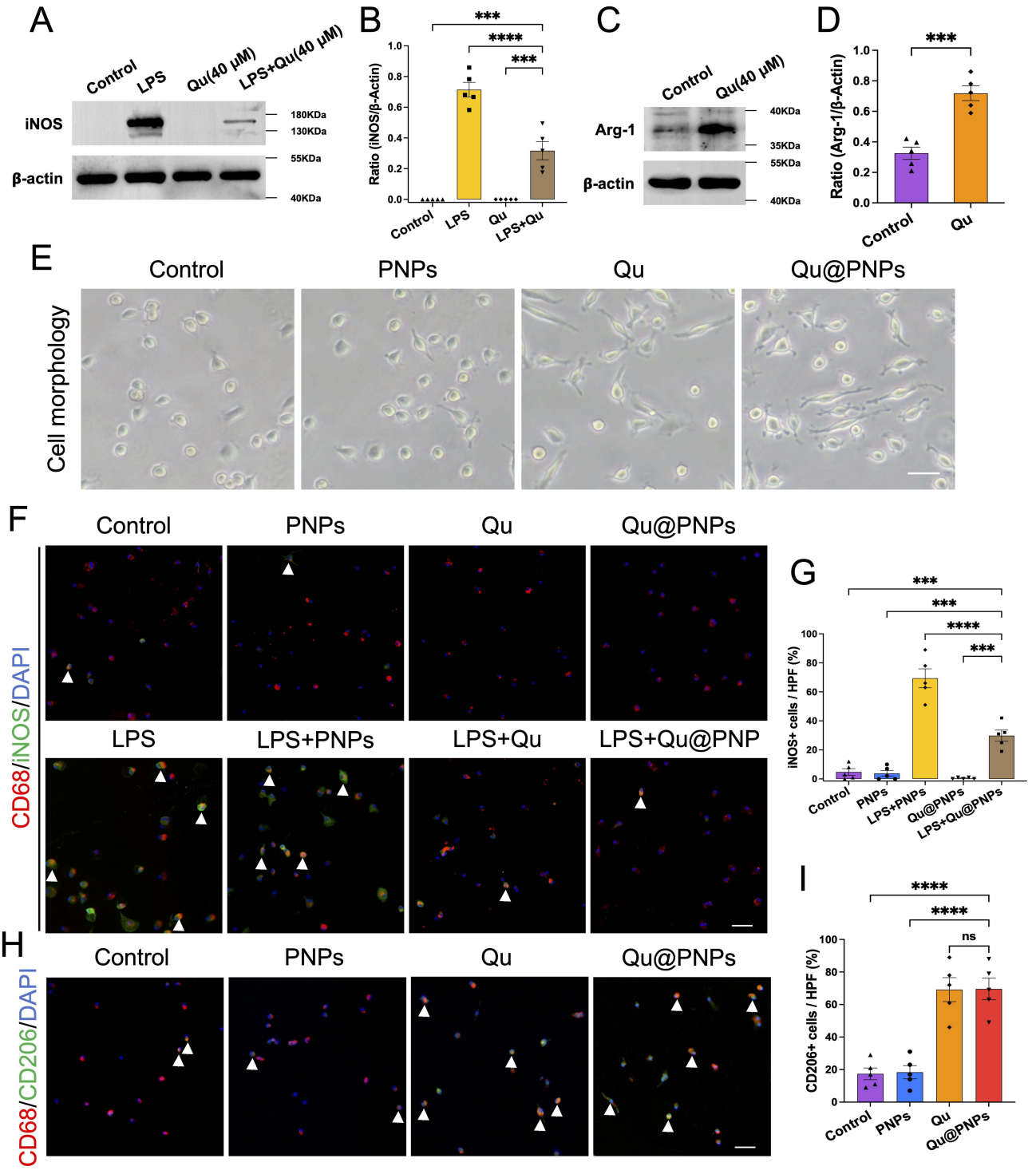

Figure 4 In vitro regulation of macrophage polarization by Qu@PNPs. (**A**) Experimental method for the LPS+Qu group: Rat BMDMs were treated with 40 μM Qu for 30 minutes, followed by 24-hour stimulation with LPS (100 ng/mL). WB analysis of iNOS protein expression in rat BMDMs. (**B**) Quantitative analysis of iNOS protein levels (n=5). (**C**) Rat BMDMs were treated with 40 μM Qu for 24 hours. WB analysis of Arg-1 protein expression. (**D**) Quantitative analysis of Arg-1 protein levels (n=5). (**E**) Microscopic images showing cell morphology changes in rat BMDMs after 24 hours of different experimental treatments, scale bar: 50 μm. (**F**) Immunofluorescence staining for iNOS expression in rat BMDMs after different treatments. Red represents CD68+ cells, green represents iNOS+ cells, and white arrows indicate CD68+iNOS+ cells, scale bar: 50 μm. (**G**) Quantitative analysis of the proportion of iNOS+ cells (n=5). (**H**) Immunofluorescence staining for CD206 expression in rat BMDMs after different treatments. Red represents CD68+ cells, green represents CD206+ cells, and white arrows indicate CD68+CD206+ cells, scale bar: 50 μm. (**I**) Quantitative analysis of the proportion of CD206+ cells (n=5). Data are presented as mean value ± standard error of the mean, *** p<0.001; **** p<0.0001; ns: not significant.

https://doi.org/10.2147/IJN.S505674

in vivo effects of Qu@PNPs on macrophage polarization and graft remodeling. Therefore, in this study, the rat subcutaneous implantation model was established to preliminarily evaluate the functionality of Qu@PNPs in the complex physiological environment and simulate the process of in vivo graft remodeling. The results showed that by day 21 post-implantation, the Qu@PNPs-dTEVG group exhibited a significant increase in M2 macrophages (co-expressing CD68 and CD206) in the graft's adventitia compared to other groups, while M1 macrophages (co-expressing CD68 and iNOS) were nearly absent (Figure 5A). Moreover, the evaluation of graft recellularization indicated that the Qu@PNPs-dTEVG group had markedly enhanced early recellularization within the graft compared to other groups (Figure 5B and F). Finally, the analysis of neovascularization (CD31+/CD31+α-SMA+) surrounding the graft revealed that the Qu@PNPs-dTEVG group exhibited a significantly higher number of new blood vessels, with immunofluorescence showing circular CD31-positive or CD31/α-SMA double-positive signals (Figure 5C and G). These findings suggest that in vivo, Qu@PNPs can regulate macrophage polarization by increasing M2 macrophages and enhancing early graft remodeling, characterized by improved graft recellularization and increased peripheral neovascularization.

Qu@PNPs Regulate Macrophage Polarization and Promote Early Recellularization and Peripheral Neovascularization of dTEVG in the AVG Model

In the rat subcutaneous implantation model, Qu@PNPs modification significantly promoted M2 macrophage polarization, early recellularization, and peripheral neovascularization, providing preliminary evidence of its positive effect on graft remodeling and regeneration in vivo. However, the subcutaneous environment differs significantly from the actual in vivo vascular transplantation environment encountered in clinical applications, particularly in AVG. Therefore, to further assess the impact of Qu@PNPs on macrophage polarization regulation and graft remodeling in a vascular transplantation setting, we established a rat cervical AVG model to closely simulate the clinical scenario where vascular grafts are used to construct hemodialysis access pathways. Similar to the subcutaneous model, Qu@PNPs demonstrated significant biological functions in the AVG model as well. On day 21, the Qu@PNPs-dTEVG group exhibited a marked increase in M2 macrophages in the adventitia of the graft, with almost no M1 macrophages, consistent with the findings from the subcutaneous model (Figure 6A). Additionally, early recellularization within the graft and peripheral neovascularization were also similar to the subcutaneous model (Figure 6B). Notably, α-SMA-positive cell infiltration was observed within the grafts of the Qu@PNPs-dTEVG group (Supplementary Figure 5). In summary, the results from both in vivo models complement each other, demonstrating the positive effect of Qu@PNPs modification in improving dTEVG remodeling in vivo, laying a foundation for future studies and clinical applications.

Discussion

Currently, dTEVG has been applied in large animal and even clinical vascular graft models, demonstrating promising outcomes. However, challenges remain in graft remodeling, particularly in recellularization.[7,15–17] To address this, we designed and developed a local drug delivery system by modifying dTEVG with drug-loaded PLGA nanoparticles to improve in vivo graft remodeling. Specifically, Qu@PNPs with excellent biocompatibility were prepared via nanoprecipitation and covalently conjugated to the dTEVG surface using the EDC/NHS method. The results showed a significant improvement in the bioavailability and sustained release capacity of Qu. In vitro experiments confirmed that Qu@PNPs effectively regulated macrophage polarization, significantly inhibiting M1 polarization while promoting M2 polarization. Similarly, in vivo experiments showed an increase in M2 macrophages around the adventitia of Qu@PNPs-dTEVG, along with significant improvements in graft remodeling, characterized by successful early recellularization and a marked increase in neovascularization around the graft.

Recellularization is not only a critical factor in promoting dTEVG remodeling and regeneration but also essential for maintaining good blood compatibility and homeostasis in vivo.[35] Early recellularization of decellularized tissues is crucial, as failure to achieve this can disrupt the balance between scaffold degradation and adaptive remodeling, ultimately leading to graft failure.[36] In our experiments, the surface modification of Qu@PNPs significantly promoted early in vivo recellularization of dTEVG, contributing positively to graft remodeling. Notably, in the rat AVG model, significant recellularization was observed in the Qu@PNPs-dTEVG group at 21 days post-implantation, including the

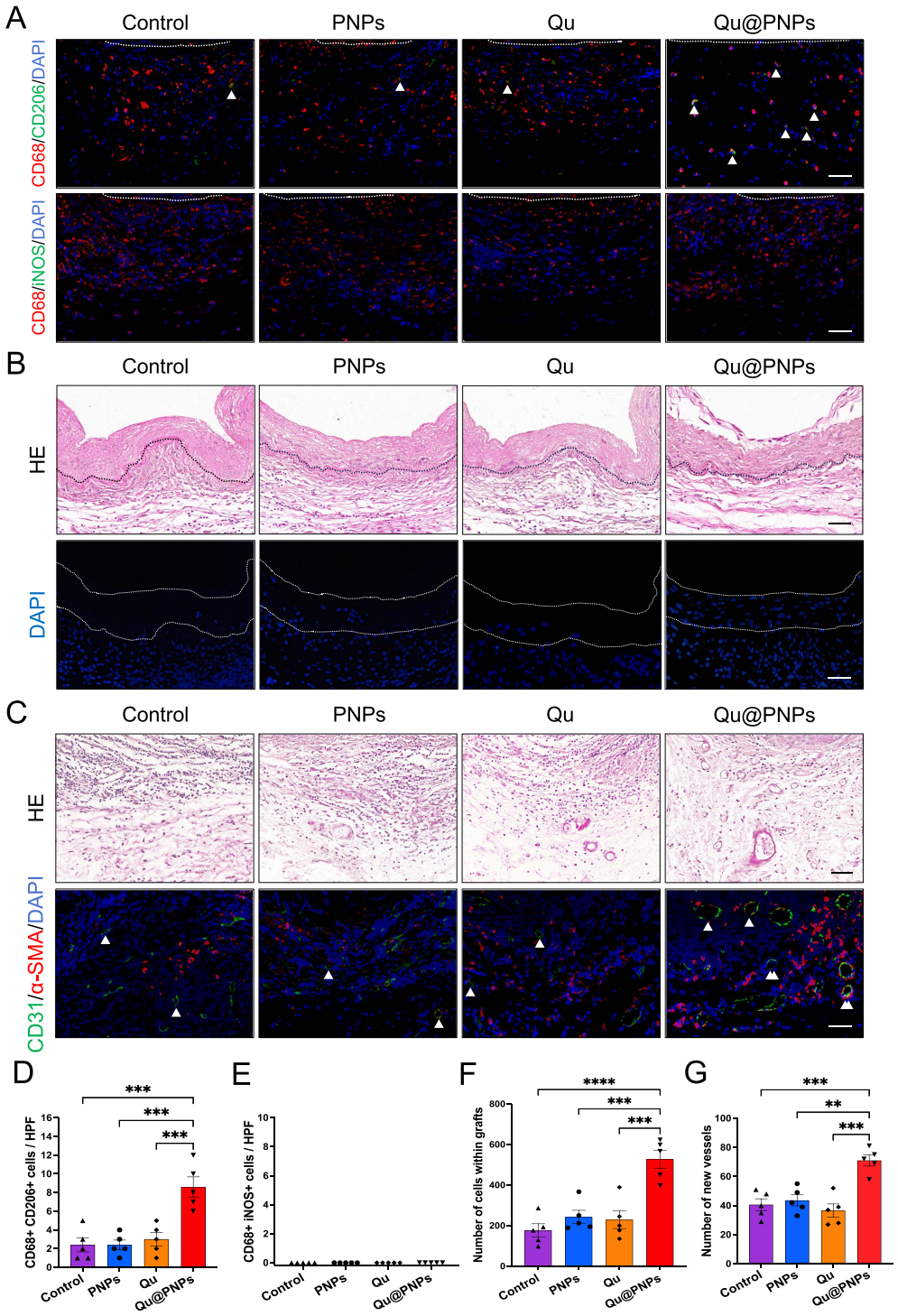

Figure 5 Qu@PNPs regulate macrophage polarization to enhance early recellularization and perivascular neovascularization in dTEVG within rat subcutaneous models. Experimental groups: Control (unmodified dTEVG), PNPs (PNPs-dTEVG), Qu (Qu-dTEVG), Qu@PNPs (Qu@PNPs-dTEVG). (**A**) Immunofluorescence detection of macrophage polarization in the graft adventitial region (below the dashed line) on day 21 in the subcutaneous implantation model. M2 macrophages (CD68+CD206+, red represents CD68+, green represents CD206+), M1 macrophages (CD68+iNOS+, red represents CD68+, green represents iNOS+), with white arrows indicating M2 macrophages, scale bar: 50 μm. (**B**) HE and DAPI fluorescence staining to assess early recellularization in the graft on day 21. In the HE staining images, the area above the black dashed line represents the graft, and in the DAPI fluorescence images, the area between the white dashed lines represents the graft, scale bar: 50 μm. (**C**) HE and immunofluorescence detection of neovascularization in the graft surrounding area on day 21. In the immunofluorescence images, white arrows indicate new blood vessels (CD31+/CD31+α-SMA+), green represents CD31+, and red represents α-SMA+, scale bar: 50 μm. (**D**) Quantitative analysis of the number of M2 macrophages (CD68 +CD206+) in the graft adventitial region (n=5). (**E**) Quantitative analysis of the number of M1 macrophages (CD68+iNOS+) in the graft adventitial region (n=5). (**F**) Quantitative analysis of early recellularization in the graft (n=5). (**G**) Quantitative analysis of the number of new blood vessels in the graft surrounding area (n=5). Data are presented as mean value ± standard error of the mean, ** p<0.01; *** p<0.001; **** p<0.0001; ns: not significant (not shown in the figure).

https://doi.org/10.2147/IJN.S505674

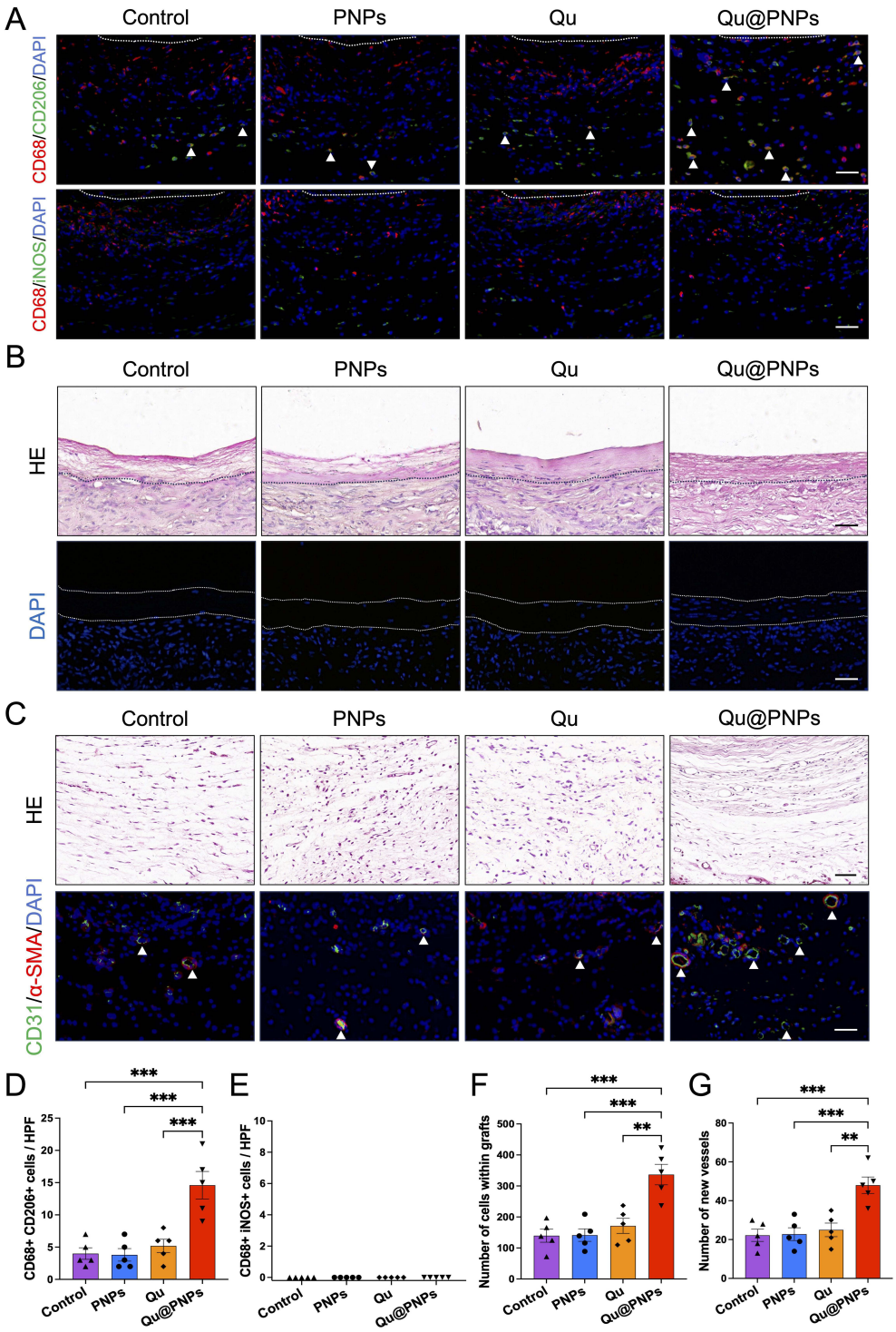

Figure 6 Qu@PNPs regulate macrophage polarization to enhance early recellularization and perivascular neovascularization in dTEVG within rat AVG models. Experimental groups: Control (unmodified dTEVG), PNPs (PNPs-dTEVG), Qu (Qu-dTEVG), Qu@PNPs (Qu@PNPs-dTEVG). (**A**) Immunofluorescence detection of macrophage polarization in the graft adventitial region (below the dashed line) in the AVG model. M2 macrophages (CD68+CD206+, red represents CD68+, green represents CD206+), M1 macrophages (CD68+iNOS+, red represents CD68+, green represents iNOS+), with white arrows indicating M2 macrophages, scale bar: 50 μm. (**B**) HE and DAPI fluorescence staining to assess early recellularization in the graft within the AVG model. In the HE staining images, the area above the black dashed line represents the graft, and in the DAPI fluorescence images, the area between the white dashed lines represents the graft, scale bar: 50 μm. (**C**) HE and immunofluorescence detection of neovascularization in the graft surrounding area on day 21. In the immunofluorescence images, white arrows indicate new blood vessels (CD31+/CD31+α-SMA +), green represents CD31+, and red represents α-SMA+, scale bar: 50 μm. (**D**) Quantitative analysis of the number of M2 macrophages (CD68+CD206+) in the graft adventitial region (n=5). (**E**) Quantitative analysis of the number of M1 macrophages (CD68+iNOS+) in the graft adventitial region (n=5). (**F**) Quantitative analysis of early recellularization in the graft (n=5). (**G**) Quantitative analysis of the number of new blood vessels in the graft surrounding area (n=5). Data are presented as mean value ± standard error of the mean, ** p<0.01; *** p<0.001; ns: not significant (not shown in the figure).

presence of α-SMA-positive smooth muscle-like cells within the graft. However, endothelialization was not yet evident in the intimal layer. This may be attributed to the specific characteristics of the AVG model we employed. The prolonged exposure to high-flow blood conditions (>600 mL/min) likely impairs endothelialization of dTEVG in the AVG context.[4] Furthermore, our previous studies have demonstrated that endothelialization of dTEVG in human AVG is highly limited, and similarly, in the rat AVG model, it requires a considerable period (approximately one year) to achieve complete endothelialization.[33] Nonetheless, our study successfully achieved early recellularization within the graft, which is particularly critical for ensuring proper healing of dTEVG after repeated punctures during hemodialysis treatment.[18,19]

Numerous studies indicate that macrophages are involved in all stages of tissue repair, from acute inflammatory response to resolution and subsequent remodeling.[37–39] Research by Breuer et al highlights that macrophages are essential for the remodeling of vascular grafts.[40,41] Depleting macrophages prior to implantation results in grafts lacking endothelial and medial layers.[41] Macrophages exhibit high plasticity and can polarize into different functional states in response to various stimuli. These states are broadly categorized into pro-inflammatory M1 macrophages and pro-regenerative M2 macrophages, which promote tissue repair and regeneration.[42] Given the modulatory potential of macrophage polarization, many studies on graft remodeling have focused on its regulation. For instance, Wang et al demonstrated in their study on biomimetic glycopeptide hydrogel-coated Polycaprolactone (PCL)/nano-Hydroxyapatite (nHA) scaffolds that promoting M2 macrophage polarization facilitated scaffold regeneration in damaged cranial bone.[43] Similarly, studies on PCL vascular graft remodeling revealed that enhancing M2 macrophage polarization promotes graft recellularization.[44] However, whether regulating M2 macrophage polarization can improve recellularization in dTEVG remains unclear. In our study, we found that modulating macrophage polarization towards the M2 phenotype significantly enhanced in vivo remodeling of dTEVG, particularly by promoting graft recellularization. Therefore, promoting M2 macrophage polarization plays a positive role in achieving favorable recellularization of dTEVG in vivo.

The vascular network plays a critical role in delivering blood, transporting oxygen, and providing nutrients at the microvascular interface.[45] Therefore, neovascularization at the microcirculation level is vital for the remodeling and regeneration of dTEVG. In our study, we observed newly formed vascular structures surrounding the dTEVG. Interestingly, the introduction of Qu@PNPs significantly increased the number of new blood vessels around the graft. This suggests that Qu may promote neovascularization. As a natural flavonoid compound, Qu has been shown to regulate macrophage polarization.[20–23] Coupled with the noticeable increase in M2 macrophages in the adventitial region of the Qu@PNPs-modified grafts, it is hypothesized that Qu may influence peripheral neovascularization through the modulation of macrophage polarization pathways. The importance of macrophages in neovascularization has been documented in previous studies, where the depletion of macrophages during the early stages of wound healing significantly impaired the formation of new blood vessels.[46] Macrophages in different polarization states have varying effects on neovascularization. While M1 macrophages initially produce high levels of VEGF after biomaterial implantation, promoting the formation of immature vascular networks, their prolonged presence can lead to the regression of these new blood vessels.[47,48] In contrast, M2 macrophages facilitate the growth, anastomosis, and maturation of new blood vessels.[49] Therefore, regulating macrophage polarization towards the M2 phenotype may represent an important mechanism for enhancing neovascularization around the graft.

In recent years, due to its excellent biological properties, Qu has increasingly been applied in tissue engineering. Functionalized Qu scaffolds have been studied and utilized in various fields, including skin and bone regeneration.[50,51] For instance, Sharma et al developed chitosan hydrogel films incorporating Qu, which showed promising skin regeneration in a full-thickness skin excision model in mice.[50] Additionally, Gupta et al co-modified decellularized goat lung scaffolds with Qu and nHA, demonstrating enhanced growth and proliferation of bone marrow-derived mesenchymal stem cells (BMMSCs) and their differentiation towards osteoblasts.[51] In our study, the application of Qu also contributed positively to graft remodeling, which is closely related to its role in promoting macrophage M2 polarization. Notably, the time-dependent nature of M2 macrophage polarization during graft remodeling has been well-recognized.[52] Previous studies attempted to regulate macrophage polarization by delivering Interleukin-4 (IL-4), but this approach has limitations such as high costs and rapid degradation.[53] Others have sought to influence M2 polarization by altering the fiber alignment of grafts to modulate macrophage mechanotransduction.[54,55] However, since dTEVG is derived from native vessels, such modifications to fiber structures are currently unfeasible. In contrast, Qu offers several advantages as a regulatory agent: it is abundant,

easily accessible, and has a high safety profile. Furthermore, the modification strategy used in our study ensures that Qu@PNPs are primarily located within the structure of dTEVG, especially in the adventitia. Interestingly, previous studies have shown that cell infiltration, particularly of monocyte-derived macrophages, primarily occurs through the adventitia in vascular grafts.[56] Therefore, this approach offers higher precision and accuracy in regulation. Taken together, the method employed in this study offers distinct advantages in promoting graft remodeling.

Although our study provides valuable insights, it has some limitations. First, the use of a single animal model limits the generalizability of the results. Due to physiological differences across species, the findings may face challenges when translating into clinical applications. Second, the observation period was relatively short, focusing primarily on the early stages of graft remodeling. The long-term stability and functionality of the grafts, particularly during later remodeling phases, still require extended observation. Additionally, as this study is observational in nature, it lacks validation of the underlying biological mechanisms. To address these limitations, future work should extend the observation period, incorporate multiple relevant animal models, and include mechanistic validation to fully elucidate the role of Qu in regulating macrophage polarization during dTEVG remodeling. This will provide a stronger theoretical and experimental foundation for the effective application of Qu, as well as offer new strategies for optimizing dTEVG design, ultimately advancing its clinical use and providing improved vascular access for hemodialysis patients.

Conclusion

In summary, this study shows that Qu@PNPs exhibit excellent biocompatibility, effectively regulate macrophage M2 polarization, and significantly improve the in vivo remodeling of dTEVG through local surface modification. This is primarily evidenced by successful early recellularization and increased peripheral neovascularization. These positive results establish a solid theoretical and experimental foundation for the effective application of Qu in vascular grafts, while also providing new insights and strategies for further optimization of dTEVG design, facilitating its future clinical translation and providing better vascular access for hemodialysis patients.

Acknowledgments

This work was supported by International (Regional) Cooperation and Exchange (ICE) Projects of the National Natural Science Foundation of China (NSFC) (grant number 82120108005) and Natural Science Foundation of Hunan Province of China (grant number 2021JJ40874, 2024JJ5466). We would like to express our gratitude to the researchers from the Institute of Vascular Diseases at Central South University for their assistance during the experiment.

Disclosure

The authors report no conflicts of interest in this work.

References

1. Chen TK, Knicely DH, Grams ME. Chronic kidney disease diagnosis and management: a review. *JAMA*. 2019;322(13):1294–1304. doi:10.1001/jama.2019.14745
2. Yang C, Wang H, Zhao X, et al. CKD in China: evolving spectrum and public health implications. *Am J Kidney Dis*. 2020;76(2):258–264. doi:10.1053/j.ajkd.2019.05.032
3. Pecoits-Filho R, Okpechi IG, Donner JA, et al. Capturing and monitoring global differences in untreated and treated end-stage kidney disease, kidney replacement therapy modality, and outcomes. *Kidney Int Suppl (2011)*. 2020;10(1):e3–e9. doi:10.1016/j.kisu.2019.11.001
4. Lok CE, Huber TS, Lee T, et al. KDOQI clinical prac tice guideline for vascular access: 2019 update. *Am J Kidney Dis*. 2020;75(4 Suppl 2):S1–S164. doi:10.1053/j.ajkd.2019.12.001
5. Lok CE, Huber TS, Orchanian-Cheff A, Rajan DK. Arteriovenous access for hemodialysis: a review. *JAMA*. 2024;331(15):1307–1317. doi:10.1001/jama.2024.0535
6. Jha V, Garcia-Garcia G, Iseki K, et al. Chronic kidney disease: global dimension and perspectives. *Lancet*. 2013;382:9888):260–72. doi:10.1016/S0140-6736(13)60687-X
7. Dahl SL, Kypson AP, Lawson JH, et al. Readily available tissue-engineered vascular grafts. *Sci Transl Med*. 2011;3(68):68ra9. doi:10.1126/scitranslmed.3001426
8. Roy-Chaudhury P, Kelly BS, Miller MA, et al. Venous neointimal hyperplasia in polytetrafluoroethylene dialysis grafts. *Kidney Int*. 2001;59(6):2325–2334. doi:10.1046/j.1523-1755.2001.00750.x
9. Akoh JA, Patel N. Infection of hemodialysis arteriovenous grafts. *J Vasc Access*. 2010;11(2):155–158. doi:10.1177/112972981001100213

10. Sandusky GE, Lantz GC, Badylak SF. Healing comparison of small intestine submucosa and ePTFE grafts in the canine carotid artery. *J Surg Res*. 1995;58(4):415–420. doi:10.1006/jsre.1995.1064
11. Xing H, Lee H, Luo L, Kyriakides TR. Extracellular matrix-derived biomaterials in engineering cell function. *Biotechnol Adv*. 2020;42:107421. doi:10.1016/j.biotechadv.2019.107421
12. Lin CH, Hsia K, Ma H, Lee H, Lu JH. In vivo performance of decellularized vascular grafts: a review article. *Int J mol Sci*. 2018;19(7):2101. doi:10.3390/ijms19072101
13. Seifu DG, Purnama A, Mequanint K, Mantovani D. Small-diameter vascular tissue engineering. *Nat Rev Cardiol*. 2013;10(7):410–421. doi:10.1038/nrcardio.2013.77
14. Choudhury D, Yee M, Sheng ZLJ, Amirul A, Naing MW. Decellularization systems and devices: state-of-the-art. *Acta Biomater*. 2020;115:51–59. doi:10.1016/j.actbio.2020.07.060
15. Das A, Smith RJ, Andreadis ST. Harnessing the potential of monocytes/macrophages to regenerate tissue-engineered vascular grafts. *Cardiovasc Res*. 2024;120(8):839–854. doi:10.1093/cvr/cvae106
16. Boer U, Spengler C, Jonigk D, et al. Coating decellularized equine carotid arteries with CCN1 improves cellular repopulation, local biocompatibility, and immune response in sheep. *Tissue Eng Part A*. 2013;19(15–16):1829–1842. doi:10.1089/ten.TEA.2012.0558
17. Spark JI, Yeluri S, Derham C, Wong YT, Leitch D. Incomplete cellular depopulation may explain the high failure rate of bovine ureteric grafts. *Br J Surg*. 2008;95(5):582–585. doi:10.1002/bjs.6052
18. Guidoin R, Canizales S, Charara J, et al. Vascular access for hemodialysis: pathologic features of surgically excised ePTFE grafts. *Ann Vasc Surg*. 1992;6(6):517–524. doi:10.1007/BF02000823
19. Tillman BW, Yazdani SK, Neff LP, et al. Bioengineered vascular access maintains structural integrity in response to arteriovenous flow and repeated needle puncture. *J Vasc Surg*. 2012;56(3):783–793. doi:10.1016/j.jvs.2012.02.030
20. Tieu S, Charchoglyan A, Wagter-Lesperance L, et al. Immunoceuticals: harnessing their immunomodulatory potential to promote health and wellness. *Nutrients*. 2022;14(19):4075. doi:10.3390/nu14194075
21. Riaz A, Ali S, Summer M, et al. Exploring the underlying pharmacological, immunomodulatory, and anti-inflammatory mechanisms of phytochemicals against wounds: a molecular insight. *Inflammopharmacology*. 2024;32(5):2695–2727. doi:10.1007/s10787-024-01545-5
22. Fan H, Tang HB, Shan LQ, et al. Quercetin prevents necroptosis of oligodendrocytes by inhibiting macrophages/microglia polarization to M1 phenotype after spinal cord injury in rats. *J Neuroinflammation*. 2019;16(1):206. doi:10.1186/s12974-019-1613-2
23. Tsai CF, Chen GW, Chen YC, et al. Regulatory effects of quercetin on M1/M2 macrophage polarization and oxidative/antioxidative balance. *Nutrients*. 2021;14(1):67. doi:10.3390/nu14010067
24. Roh JD, Sawh-Martinez R, Brennan MP, et al. Tissue-engineered vascular grafts transform into mature blood vessels via an inflammation-mediated process of vascular remodeling. *Proc Natl Acad Sci U S A*. 2010;107(10):4669–4674. doi:10.1073/pnas.0911465107
25. Smith RJ Jr, Nasiri B, Kann J, et al. Endothelialization of arterial vascular grafts by circulating monocytes. *Nat Commun*. 2020;11(1):1622. doi:10.1038/s41467-020-15361-2
26. Wang W, Sun C, Mao L, et al. The biological activities, chemical stability, metabolism and delivery systems of quercetin: a review. *Trends Food Sci Technol*. 2016;56:21–38. doi:10.1016/j.tifs.2016.07.004
27. Tran TH, Guo Y, Song D, Bruno RS, Lu X. Quercetin-containing self-nanoemulsifying drug delivery system for improving oral bioavailability. *J Pharm Sci*. 2014;103(3):840–852. doi:10.1002/jps.23858
28. Niu X, Zou W, Liu C, Zhang N, Fu C. Modified nanoprecipitation method to fabricate DNA-loaded PLGA nanoparticles. *Drug Dev Ind Pharm*. 2009;35(11):1375–1383. doi:10.3109/03639040902939221
29. Goodarzi H, Jadidi K, Pourmotabed S, Sharifi E, Aghamollaei H. Preparation and in vitro characterization of cross-linked collagen-gelatin hydrogel using EDC/NHS for corneal tissue engineering applications. *Int J Biol Macromol*. 2019;126:620–632. doi:10.1016/j.ijbiomac.2018.12.125
30. Zhong H, Chan G, Hu Y, Hu H, Ouyang D. A comprehensive map of FDA-approved pharmaceutical products. *Pharmaceutics*. 2018;10(4):263. doi:10.3390/pharmaceutics10040263
31. Ghitman J, Biru EI, Stan R, Iovu H. Review of hybrid PLGA nanoparticles: future of smart drug delivery and theranostics medicine. *Mater Des*. 2020;193:108805. doi:10.1016/j.matdes.2020.108805
32. Seegobin N, Abdalla Y, Li G, Murdan S, Shorthouse D, Basit AW. Optimising the production of PLGA nanoparticles by combining design of experiment and machine learning. *Int J Pharm*. 2024;667:124905. doi:10.1016/j.ijpharm.2024.124905
33. Wang T, Lu P, Wan Z, et al. Adaptation process of decellularized vascular grafts as hemodialysis access in vivo. *Regen Biomater*. 2024:11:rbae029. doi:10.1093/rb/rbae029.
34. Li H, Cao Z, Liu C, et al. Quercetin inhibits neuronal pyroptosis and ferroptosis by modulating microglial M1/M2 polarization in atherosclerosis. *J Agric Food Chem*. 2024;72(21):12156–12170. doi:10.1021/acs.jafc.4c01134
35. Xie J, Wan J, Tang X, Li W, Peng B. Heparin modification improves the re-endothelialization and angiogenesis of decellularized kidney scaffolds through antithrombosis and anti-inflammation in vivo. *Transl Androl Urol*. 2021;10(9):3656–3668. doi:10.21037/tau-21-703
36. Wu Y, Chen X, Song P, et al. Functional oxidized hyaluronic acid cross-linked decellularized heart valves for improved immunomodulation, anti-calcification, and recellularization. *Adv Healthc Mater*. 2024;13(16):e2303737. doi:10.1002/adhm.202303737
37. Raziyeva K, Kim Y, Zharkinbekov Z, Kassymbek K, Jimi S, Saparov A. Immunology of Acute and Chronic Wound Healing. *Biomolecules*. 2021;11(5):700. doi:10.3390/biom11050700
38. Hassanshahi A, Moradzad M, Ghalamkari S, Fadaei M, Cowin AJ, Hassanshahi M. Macrophage-mediated inflammation in skin wound healing. *Cells*. 2022;11(19):2953. doi:10.3390/cells11192953
39. Kloc M, Ghobrial RM, Wosik J, Lewicka A, Lewicki S, Kubiak JZ. Macrophage functions in wound healing. *J Tissue Eng Regen Med*. 2019;13(1):99–109. doi:10.1002/term.2772
40. Hibino N, Mejias D, Pietris N, et al. The innate immune system contributes to tissue-engineered vascular graft performance. *FASEB J*. 2015;29(6):2431–2438. doi:10.1096/fj.14-268334
41. Hibino N, Yi T, Duncan DR, et al. A critical role for macrophages in neovessel formation and the development of stenosis in tissue-engineered vascular grafts. *FASEB J*. 2011;25(12):4253–4263. doi:10.1096/fj.11-186585
42. Liu YC, Zou XB, Chai YF, Yao YM. Macrophage polarization in inflammatory diseases. *Int J Biol Sci*. 2014;10(5):520–529. doi:10.7150/ijbs.8879

43. Wang Y, Wang J, Gao R, et al. Biomimetic glycopeptide hydrogel coated PCL/nHA scaffold for enhanced cranial bone regeneration via macrophage M2 polarization-induced osteo-immunomodulation. *Biomaterials*. 2022;285:121538. doi:10.1016/j.biomaterials.2022.121538
44. Wang Z, Cui Y, Wang J, et al. The effect of thick fibers and large pores of electrospun poly(ε-caprolactone) vascular grafts on macrophage polarization and arterial regeneration. *Biomaterials*. 2014;35(22):5700–5710. doi:10.1016/j.biomaterials.2014.03.078
45. Sun X, Altalhi W, Nunes SS. Vascularization strategies of engineered tissues and their application in cardiac regeneration. *Adv Drug Deliv Rev*. 2016;96:183–194. doi:10.1016/j.addr.2015.06.001
46. Aurora AB, Porrello ER, Tan W, et al. Macrophages are required for neonatal heart regeneration. *J Clin Invest*. 2014;124(3):1382–1392. doi:10.1172/jci72181
47. Dondossola E, Holzapfel BM, Alexander S, Filippini S, Hutmacher DW, Friedl P. Examination of the foreign body response to biomaterials by nonlinear intravital microscopy. *Nat Biomed Eng*. 2016;1(1). doi:10.1038/s41551-016-0007
48. Graney PL, Ben-Shaul S, Landau S, et al. Macrophages of diverse phenotypes drive vascularization of engineered tissues. *Sci Adv*. 2020;6(18): eaay6391. doi:10.1126/sciadv.aay6391
49. Zarubova J, Hasani-Sadrabadi MM, Ardehali R, Li S. Immunoengineering strategies to enhance vascularization and tissue regeneration. *Adv Drug Deliv Rev*. 2022;184:114233. doi:10.1016/j.addr.2022.114233
50. Sharma G, George Joy J, Sharma AR, Kim JC. Accelerated full-thickness skin wound tissue regeneration by self-crosslinked chitosan hydrogel films reinforced by oxidized CNC-AgNPs stabilized Pickering emulsion for quercetin delivery. *J Nanobiotechnology*. 2024;22(1):323. doi:10.1186/s12951-024-02596-0
51. Gupta SK, Kumar R, Mishra NC. Influence of quercetin and nanohydroxyapatite modifications of decellularized goat-lung scaffold for bone regeneration. *Mater Sci Eng C Mater Biol Appl*. 2017;71:919–928. doi:10.1016/j.msec.2016.10.085
52. Zhang F, King MW. Immunomodulation strategies for the successful regeneration of a tissue-engineered vascular graft. *Adv Healthc Mater*. 2022;11 (12):e2200045. doi:10.1002/adhm.202200045
53. Bonito V, Koch SE, Krebber MM, et al. Distinct effects of heparin and interleukin-4 functionalization on macrophage polarization and in situ arterial tissue regeneration using resorbable supramolecular vascular grafts in rats. *Adv. Healthcare Mater*. 2021;10(21):2101103. doi:10.1002/adhm.202101103
54. Song J, Huang S, Linghu X, et al. 3D printing of different fibres towards HA/PCL scaffolding induces macrophage polarization and promotes osteogenic differentiation of BMSCs. *PLoS One*. 2025;20(1):e0314150. doi:10.1371/journal.pone.0314150
55. Schoenenberger AD, Tempfer H, Lehner C, et al. Macromechanics and polycaprolactone fiber organization drive macrophage polarization and regulate inflammatory activation of tendon in vitro and in vivo. *Biomaterials*. 2020;249:120034. doi:10.1016/j.biomaterials.2020.120034
56. Kirkton RD, Santiago-Maysonet M, Lawson JH, et al. Bioengineered human acellular vessels recellularize and evolve into living blood vessels after human implantation. *Sci Transl Med*. 2019;11(485). doi:10.1126/scitranslmed.aau6934